True near field versus contrast near field imaging.

Jean-Baptiste Masson, Guilhem Gallot

True near field versus contrast near field imaging

Jean-Baptiste Masson and Guilhem Gallot

Laboratoire d'Optique et Biosciences, Ecole Polytechnique, CNRS UMR 7645, INSERM U696
91128 Palaiseau, France

Jean-Baptiste.Masson@polytechnique.edu

Guilhem.Gallot@polytechnique.edu

Abstract: We demonstrate that in near field imaging, interaction between light and sample can be divided into two main areas: the true near field and the contrast near field domain. We performed extensive numerical simulations in order to identify the limits of these areas, and to investigate contrast near field imaging in which much easier propagation calculation can be achieved. Finally, we show an application with terahertz axonal imaging.

OCIS codes: 110.0180 Microscopy, 260.1960 Diffraction Theory, 260.3090 Infrared, far

References and links

1. A. Lewis, H. Taha, A. Strinkovski, A. Manevitch, A. Khatchatouriants, R. Dekhter and E. Ammann, "Near-field optics: from subwavelength illumination to nanometric shadowing ," Nature biotechnology **21,** 1378–1386 (2003).
2. Y. Lu, T. Wei, F. Duewer, Y. Lu, N.-B Ming, P. G. Schultz, and X.-D. Xiang, "Nondestructive Imaging of Dielectric-Constant Profiles and Ferroelectric Domains with a Scanning-Tip Microwave Near-Field Microscope," Science **276,** 2004–2006 (1997).
3. D. Marks and P.S. Carney, "Near-field diffractive elements," Opt. Lett. **30,** 1870–1872 (2005).
4. S.I. Bozhevolnyi and B.Vohnsen,"Near-Field Optical Holography," Phys. Rev. Lett. **77,** 3351 (1996).
5. M. Naruse, T. Yatsui, W. Nomura, N. Hirose, M. Ohtsu , "Hierarchy in optical near-fields and its application to memory retrieval," Opt. Express **13,** 23, 9265–9271 (2005), http://www.opticsexpress.org/abstract.cfm?id=86211
6. D. Molenda, G. Colas des Francs, U. C. Fischer, N. Rau, A. Naber , "High-resolution mapping of the optical near-field components at a triangular nano-aperture," Opt. Express **26,** 23, 10688–10696 (2005), http://www.opticsexpress.org/abstract.cfm?id=86673
7. Comsol, Comsol Inc., Burlington, MA.
8. M. A. Bhatti,"Fundamental Finite Element Analysis and Applications: With Mathematica and Matlab Computations,"(J. Wiley & Sons,) (2005)
9. M. Golosovsky, E. Maniv, D. Davidov and A. Frenkel, "Near-Field of a Scanning Aperture Microwave Probe: A 3-D Finite Element Analysis," IEEE. Trans. Instr. Meas. **51,** 1090 (2002).
10. J.-B. Masson and G. Gallot , "Coupling between surface plasmons in subwavelength hole arrays," Phys. Rev. B. **73,** (2006).
11. J.-B Masson, M.-P Sauviat, J.-L Martin and G. Gallot, "Ionic contrast terahertz near field imaging of axonal water fluxes," Proc. Natl. Acad. Sci. USA **103,** 4808–4812 (2006).
12. M. Born, E. Wolf , "Principles of Optics" , (Cambridge Univ. Press, Cambridge, U.K.), 6th Ed. (1997)
13. H.A. Bethe , "Theory of diffraction by small holes," Phys. Rev. **66,** 163–182 (1944).
14. R.E. English, Jr., and N. George , "Diffraction from a small square aperture: approximate aperture fields," J. Opt. Soc. Am. A **5,** No. 2 (1988).
15. P. Y. Han, G. C. Cho, and X.-C. Zhang , "Time-domain transillumination of biological tissues with terahertz pulses," Opt. Lett. **25,** no 4 3009 (2004).
16. M.C. Beard, G.M. Turner and C.A. Schmuttenmaer, "Progress towards two-dimensional biomedical imaging with THz spectroscopy," Phys. Med. Biol. **47,** 3841-3846 (2002).
17. A.J. Fitzgerald, E. Berry, N.N. Zinov'ev, S. Homer-vanniasinkam, R.E. Miles, J.M. Chamberlain and M.A. Smith ,"Catalogue Of Human Tissue Optical Properties At Terahertz Frequencies," J. Biol. Phys **29,** 123–128 (2003).

#73200 - $15.00 USD Received 21 July 2006; accepted 16 October 2006

18. H.T. Chen, R. K., and G. C. Cho , "Terahertz imaging with nanometer resolution," Appl. Phys. Lett. **83,** 3009 (2003).
19. K. Wang, A. Barkan, and D. M. Mittleman , "Propagation effects in apertureless near-field optical antennas," Appl. Phys. Lett. **84,** 2 (2003).
20. R.S. Decca, H.D. Drew and K.L. Empson, "Investigation of the electric-field distribution at the subwavelength aperture of a near-field scanning optical microscope," Appl. Phys. Lett. **70,** (15) (1997).

1. Introduction

Near field optics offers the possibility of imaging with a precision much better than the wavelength of the electromagnetic radiation employed [1, 2, 3, 4, 5, 6]. In any near field optical system an electromagnetic wave is constrained to propagate in a volume of characteristic size smaller than the wavelength. Therefore, light emerging from this spatially constraining system has a higher spatial frequency, and then is able to image with subwavelength precision.

Mutual effect of induced electromagnetic fields on both probe and sample is at the core of near field interaction. In Far Field (FF) imaging, the sample does not modify the field around the probe. On the contrary, in near field imaging the sample alters the electromagnetic limit conditions at the probe and thus transforms the field.

These interactions are the source of the complexity of near field analysis and a reason why finite element programming [7, 8, 9, 10] are used in near field interaction. Complete analysis of experimental work is often impossible and near field imaging would profit from a simpler method of analyze. Then, is there a domain where spatial enhancement of near field imaging can be used, and where the sample does not strongly modify the field in the probe?

In this paper we demonstrate the existence of two specific processes in near field imaging, namely True Near Field (TNF) imaging and Contrast Near Field (CNF) imaging. In TNF imaging, probe and sample have strong and complex interactions, thus analyzing the electromagnetic field propagation can only be done by three dimensional (3D) finite element programming. In CNF imaging, the effect of the sample on the probe allows approximations on the field propagation around the probe and then offers a much simpler and faster way to model the signal. Analyzing a CNF experiment is then performed in two steps: first, a full 3D finite element programming is locally performed to evaluate the electric field in the probe alone, and second, this field is propagated by Green functions through the sample. We performed extensive finite element programming in order to characterize both processes. Finally, we show an application in terahertz near field imaging of axons.

2. Simulation model and results

Near field interactions have been studied with two different methods of simulation. First, we carried out the direct resolution of Maxwell's equations through full 3D *ab initio* finite element (FEM) analysis method of the electric field propagation through the aperture and the sample [8, 9, 11, 10]. This method provides quantitative information on the field distribution in the probe and all over the sample. Our work is focused on near field imaging with aperture, but results can be extended to apertureless near field imaging, *i.e.* imaging with a tip. Large sets of parameters have been tested to fully characterize the aperture properties: values from 50 to 10^6 for both real and imaginary part of the relative permittivity, or values from 10^2 to 10^{10} for the conductivity have been tested (values are given in Gaussian units). Results differ from negligible quantities in all simulations. All theses values cover characteristics of metals and dielec trics from the visible to the terahertz range.

Second, the resolution of Maxwell's equation was carried out with 3D FEM on the aperture alone. Then, the electric field in the aperture is extracted. Classic scalar Green functions [12] are used to propagate the electric field from the aperture through the sample to the detection

#73200 - $15.00 USD Received 21 July 2006; accepted 16 October 2006

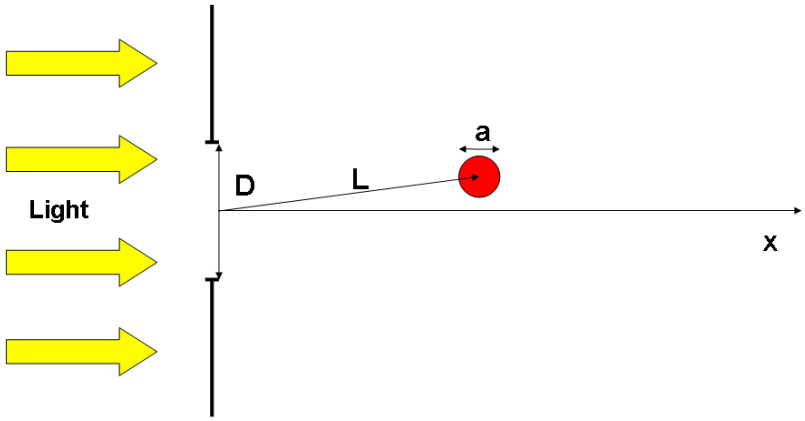

Fig. 1. Principle of near field imaging with aperture

domain. The propagation is calculated by the convolution between the Green functions and the field in the hole at the point where the field is detected. This method is called the Green Function Propagation (GFP) method.

Trying to find out general considerations was a major purpose of this study. Numerous simulations have been performed with large sets of shape and size for both apertures and samples. Only simulations with circular aperture of diameter *D* and spherical samples of diameter *a* are detailed here (Figure 1). Results of the model confirmed that, for most sample with a compact topology (no holes in the sample) and for most aperture, the relevant variables are the characteristic size of the sample and the aperture.

As our interest is focused on near field interactions, special care was provided to the mesh. In each simulations typical mesh size was $\lambda/700$ inside the aperture and near the sample, and was $\lambda/5$ in the rest of the box of simulation, with λ being the wavelength of the electromagnetic field in vacuum. Another very important point is that theoretical calculations [13, 14] show that in subwavelength aperture, the electric field diverges near the edges. When the propagation of electromagnetic field is studied with FEM programming, the volume studied is meshed, and then the field is propagated from one piece of the mesh to another. The mesh is generated with a specific mean value of point to point distance. This mean distance corresponds to the electromagnetic field spatial precision. Inside the subwavelength aperture, the maximum electric field value is correlated to the mesh size, so the mesh has to be locked inside the hole in order to compare different simulations. Furthermore, when the sample is put close to the aperture, the mesh geometry might be modified, generating artificial strong field domains, with consequences on the simulation validity. All meshes used in all simulations have been specifically prepared to keep the mean point to point distance constant inside and near the aperture, and locked to avoid strong wrapping when samples are put near the aperture. Finally, a program was designed to detect anomalous strong field domain and reject these simulations.

Two parameters are defined to understand near field interactions. The first one is linked to the physical detection, and is the difference Δ between the electric fields calculated by 3D FEM

#73200 - $15.00 USD Received 21 July 2006; accepted 16 October 2006

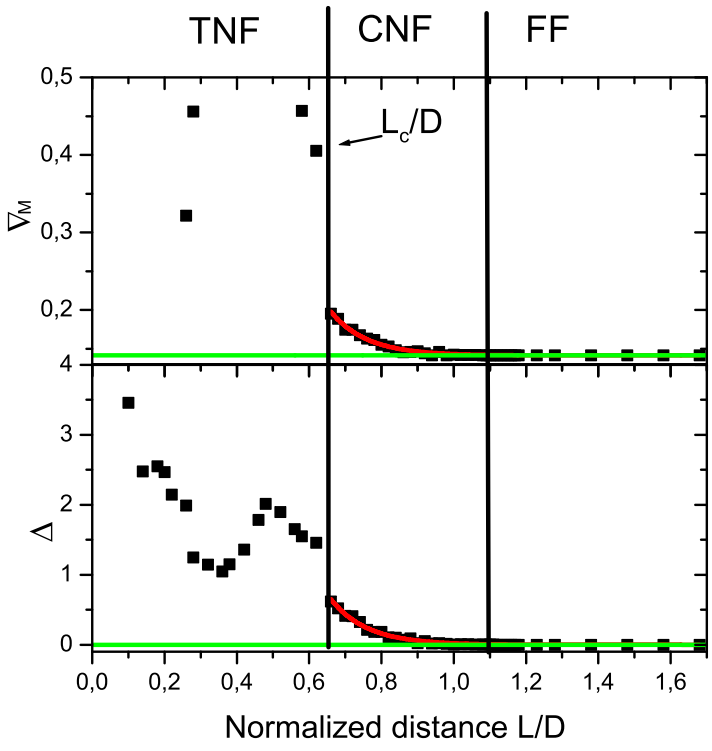

Fig. 2. Example for a spherical sample of normalized size 0.2 of the evolution of ∇_M and Δ with normalized distance L/D. Three domains have been pointed out: the true near field domain (TNF), the contrast near field domain (CNF), and the far field domain (FF). The red lines are the exponential fits in the CNF domain. The green lines are FF references.

method and GFP at the detection point in the far field domain. The second one is linked to the very structure of near field interaction and is the maximal electric field gradient ∇_M inside the aperture. An example of the evolution of Δ and ∇_M with respect to the distance L between the sample and the aperture is shown in Figure 2. For purpose of generality, most distances are normalized to the aperture size.

Three domains are observable: a domain where Δ is almost null, and where the difference between ∇_M and ∇_M^o, the value of ∇_M with no sample, is negligible. This domain corresponds to the FF domain. As the distance decreases, Δ and ∇_M differ from their FF values. First, the evolution of both parameters is monotone, the limit of this domain is the distance L_c (where Δ can no longer be approximated 0 or ∇_M to ∇_M^o). The behavior of Δ and ∇_M is no longer monotone when $L < L_c$ and corresponds to a third domain appears as the distance keeps on decreasing, characterized by a more complex behavior. In all simulations similar behavior for both parameters have been encountered. To further investigate the limit and the behavior of the electric field in the two near field domains, we studied the evolution of L_c versus a/D and D/λ (Figure 3), and the evolution of $nabla_M$ and Δ versus D/λ, a/D, and the normalized shifted distance $d = (L - L_c)/D$ (Figure 4). It should be noticed that L_c and ∇_M are independent of

#73200 - $15.00 USD Received 21 July 2006; accepted 16 October 2006

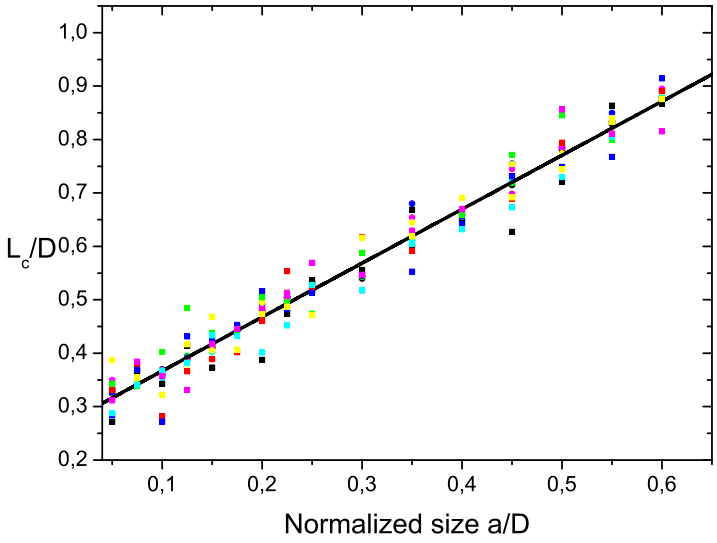

Fig. 3. Evolution of the normalized distance L_c/D versus a/D. The point color is related to D/λ: black for $1/3$, red for $1/4$, green for $1/5$, blue for $1/6$, cyan for $1/7$, magenta for $1/8$, yellow for $1/9$. The black line is the linear fit of the simulations. The shape of points is related to the simulation, circles for ∇_M and squares for Δ

the aperture and sample size in all simulations. L_c has exactly the same behavior whether it is extracted from Δ or ∇_M data, and is a linear function of the normalized size of the sample. When $L > L_c$ the evolution of both ∇_M and Δ is a decreasing exponential function of d, with a characteristic distance $D/10$.

Results on L_c and ∇_M confirm the existence of two domains in near field interactions. From the limit of FF domain to the distance L_c, it is the CNF interaction domain. In this part of space, ∇_M can be approximated to ∇_M^o and Δ to 0. In a more physical matter, in this domain the sample "feels" the near field effect of the aperture, but modifies only slightly the electric field in the aperture. So there can be a separation between the field evaluation in the hole and the field propagation through the sample.

Inside the domain limited by a sphere centered on the aperture and of radius L_c, differences between 3D FEM analysis and GFP analysis become strong and very dependent on the size and the shape of both the aperture and the sample. This domain is the TNF interaction domain. Modeling in TNF domain can only be made with FEM analysis. The interactions between the sample and the aperture are strong and complex, the sample modifies the electric field inside the aperture, changing both its intensity and shape, avoiding a GFP analysis of the experiment. One may notice that this great sensitivity is the reason why ∇_M can not describe the TNF interaction behavior.

One conclusion is that Δ and ∇_M have a correlated behavior, a criterion used on one of them can be applied to the other. But Δ is far more sensitive to geometric variations, and is also sensitive to the nature of the near field experiment. It was found that ∇_M is more stable to geometric variations, simpler to analyze, and equally linked to near field interaction.

Finally as neither Δ nor ∇_M can describe near field interaction in the TNF domain, a param-

#73200 - $15.00 USD Received 21 July 2006; accepted 16 October 2006

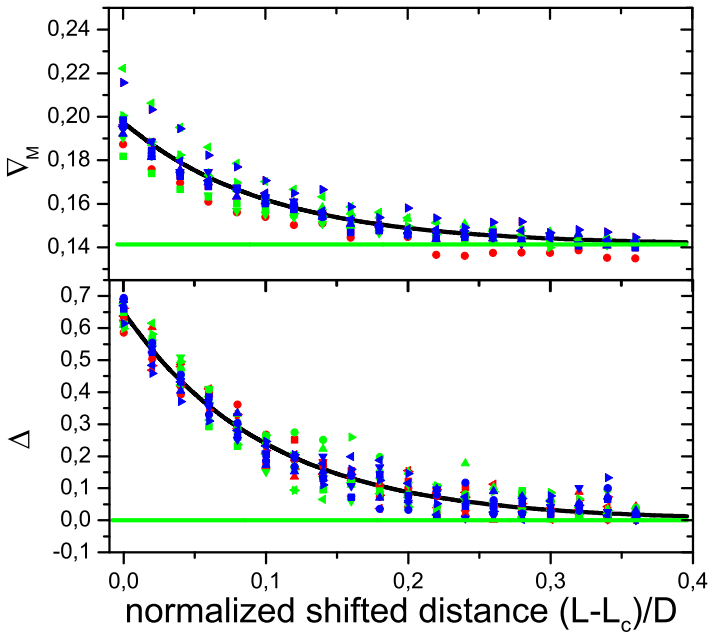

Fig. 4. Evolution of ∇_M and Δ with the normalized displacement distance $(L-L_c)/D$, for 3 aperture sizes: $\lambda/3$ (red), $\lambda/6$ (green), $\lambda/10$ (blue). For each aperture size 6 values of a/D are calculated: 0.05 (circle), 0.1 (square), 0.15 (up triangle),0.2 (down triangle),0.4 (left triangle), 0.5 (right triangle). The black line is the exponential fit of the simulation data and the green line is the FF value. On both fits the characteristic distance of the exponential is $D/10$.

eter related to the spatial electric field topology should be used. The number of extrema of the electric field N was one of the parameters considered. When the sample is in the CNF or FF domains N is equal to 1 (Figure 5). In the TNF domain, all samples modify strongly the electric field in the aperture and $N > 1$. This parameter quantitatively describes the effect of the sample on the field in the hole, more precisely it characterizes the topology changes of the electric field.

The limit between the $N = 1$ domain and the $N > 1$ is also found to be very close to L_c, confirming that L_c is the frontier between TNF and CNF domain. It illustrates the link between electric field topology in the aperture (N), electric field characteristic changes in the aperture (∇_M) and differences between 3D FEM and GFP programming (Δ).

3. Applications

The concepts previously described have been applied to terahertz imaging [11, 15, 16, 17], and more precisely terahertz axons imaging. It has been recently proved that the high sensitivity of terahertz radiation to ion concentration could be used in axon imaging [11]. Most Axons are small compared to terahertz wavelength. Therefore, near field optics is necessary. However, the reduction of the aperture size is limited by the available experimental signal to noise ratio, and by the strong absorption by water (100 μm of water absorbs approximately 50% of the signal at 1 THz). Therefore, a compromise has to be found between precision and detection.

#73200 - $15.00 USD Received 21 July 2006; accepted 16 October 2006

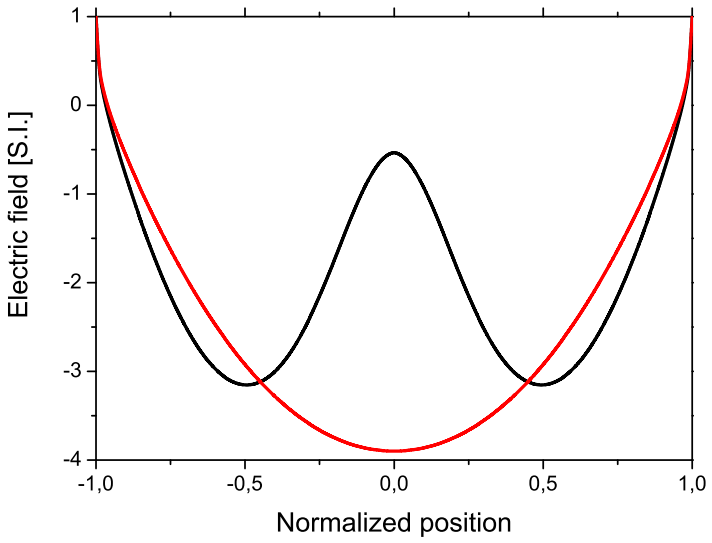

Fig. 5. Evolution of the normalized electric field (along incident polarization) in the hole with the normalized position, when the sample is in the TNF domain (black), and in the CNF domain (red). On both curves the sample is centered aperture.

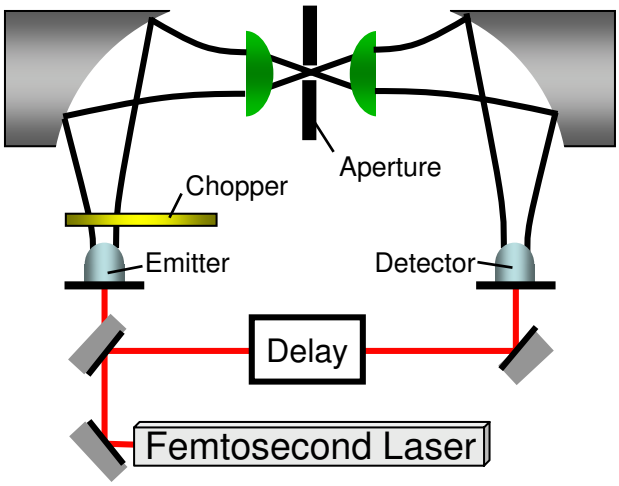

Fig. 6. Experimental setup. Terahertz generation and detection with photoconductive antenna. A femtosecond pulse generates terahertz pulses, which propagate through the subwavelength aperture and sample, and which are detected in amplitude by the detector antenna.

#73200 - $15.00 USD
Received 21 July 2006; accepted 16 October 2006

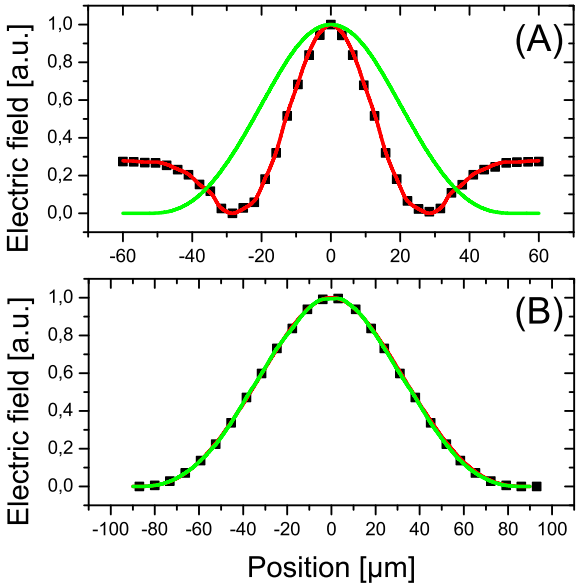

Fig. 7. Evolution of the normalized transmitted electric field versus the axon position in TNF conditions (**A**, L=80 μm) and with CNF conditions (**B**, L=140 μm)). The black dots are the experimental data, the red line is the full 3D FEM simulation fit, and the green line is the GFP fit.

We have performed experiments with broadband linearly polarized subpicosecond single cycle pulses of terahertz radiation, generated and coherently detected by illuminating photoconductive antennas with two synchronized femtosecond laser pulses (Fig. 6). Near-field microscopy with aperture was performed by focusing the terahertz radiation with a hyperhemispherical Teflon lens onto a subwavelength-diameter hole (100 μm). A neural tube of earth worm plunged in a Ringer solution [11] was put behind the aperture, then the transmitted terahertz radiation was focused by another hemispherical lens to the photoconductive detector. The imaging process consisted on moving the neural tube in front of the aperture, and measuring the transmitted electric field for each position. In a first experiment the neural tube is put closely after the aperture (80 μm), in a second one the neural tube is put 140 μm after it. Results are on Figure **??**A and 7B. All results were analyzed using the two methods described before: we performed a full 3D FEM analysis of the complete near field setup as well as GFP analysis. Both fits are shown on Figure 7. The difference between TNF and CNF is easily noticeable in the first experiment, only the complete simulation with finite element can fit the data. So a complete set of simulations is required to find physical quantities, such as the axon diameter. On the contrary the second experiment is well fitted by both methods. The fits are almost identical. However, the second fitting method is much simpler. With this method only one simple simulation followed by Green function propagation and geometrical optimization is necessary to extract physical quantities. The results are consistent with the theoretical value of L_c, found to be 105 μm. Therefore, it is more useful here to keep the distance between the sample and the probe in the C NF domain in order to get a very simple signal to analyze. Using this method we have been able to measure the axon size of the sample at $78 \pm 1\,\mu$m. Furthermore, we measured

#73200 - $15.00 USD Received 21 July 2006; accepted 16 October 2006

axon diameter variations, due to axonal water swelling, with a relative precision of 0.001 using the contrast near field imaging and the analysis cited before [11].

4. Conclusion

In this paper we have showed that in near field interaction, two domains can be separated: true near field domain and contrast near field domain. In the true near field domain, both probe and sample strongly interact, and the field in the probe is altered by the sample. In contrast near field domain, near field interactions still enhance spatial resolution, but the sample has a small effect on the field in the aperture. Analyzing an experiment in true near field conditions implies a full 3D FEM simulation. On the contrary, analyzing an experiment in contrast near field conditions, implies only a full 3D FEM simulation of the probe, followed by simple Green function propagation of the field on the probe over the model of the sample. It is a much simpler and a much faster way to analyze the data and it offers the possibility of extracting precise physical quantities from near field experiments.

#73200 - $15.00 USD Received 21 July 2006; accepted 16 October 2006